THE JOURNAL OF BIOLOGICAL CHEMISTRY VOL. 289, NO. 15, pp. 10660–10667, April 11, 2014
Published in the U.S.A.

# A Proposed Mechanism for the Promotion of Prion Conversion Involving a Strictly Conserved Tyrosine Residue in the $\beta_2$-$\alpha_2$ Loop of $PrP^{C*}$

Received for publication, January 9, 2014, and in revised form, February 27, 2014 Published, JBC Papers in Press, March 4, 2014, DOI 10.1074/jbc.M114.549030

**Timothy D. Kurt[‡], Lin Jiang[§], Cyrus Bett[‡], David Eisenberg[§], and Christina J. Sigurdson[‡¶1]**

*From the [‡]Departments of Pathology and Medicine, University of California San Diego, La Jolla, California 92093, the [§]Department of Energy Institute for Genomics and Proteomics, Howard Hughes Medical Institute, and Molecular Biology Institute, UCLA, Los Angeles, California 90095, and the [¶]Department of Pathology, Immunology, and Microbiology, University of California, Davis, California 95616*

**Background:** Single residue differences can block conversion of the cellular prion protein (PrP) to the pathogenic conformation.
**Results:** Prion conversion was reduced by non-aromatic amino acids at PrP position 169 in the $\beta_2$-$\alpha_2$ loop.
**Conclusion:** The conserved tyrosine side chain at PrP position 169 promotes efficient prion formation.
**Significance:** These findings are consistent with a steric zipper model of prion conversion.

**The transmission of infectious prions into different host species requires compatible prion protein (PrP) primary structures, and even one heterologous residue at a pivotal position can block prion infection. Mapping the key amino acid positions that govern cross-species prion conversion has not yet been possible, although certain residue positions have been identified as restrictive, including residues in the $\beta_2$-$\alpha_2$ loop region of PrP. To further define how $\beta_2$-$\alpha_2$ residues impact conversion, we investigated residue substitutions in $PrP^C$ using an *in vitro* prion conversion assay. Within the $\beta_2$-$\alpha_2$ loop, a tyrosine residue at position 169 is strictly conserved among mammals, and transgenic mice expressing mouse PrP having the Y169G, S170N, and N174T substitutions resist prion infection. To better understand the structural requirements of specific residues for conversion initiated by mouse prions, we substituted a diverse array of amino acids at position 169 of PrP. We found that the substitution of glycine, leucine, or glutamine at position 169 reduced conversion by ~75%. In contrast, replacing tyrosine 169 with either of the bulky, aromatic residues, phenylalanine or tryptophan, supported efficient prion conversion. We propose a model based on a requirement for tightly interdigitating complementary amino acid side chains within specific domains of adjacent PrP molecules, known as "steric zippers," to explain these results. Collectively, these studies suggest that an aromatic residue at position 169 supports efficient prion conversion.**

Infectious prions can be transmitted to individuals expressing the same $PrP^{C}$[2] sequence, yet interspecies transmission to hosts expressing a different $PrP^C$ sequence requires overcoming a transmission barrier. Nevertheless, during the bovine spongiform encephalopathy epidemic, interspecies prion transmission led to infection of at least 15 species, including exotic bovids, felids, non-human primates, and humans (1–4). Chronic wasting disease prions from elk and deer readily cause infection of other cervid species (5–9), yet the risk of spread to humans, livestock, or other wildlife remains unclear. Identifying the molecular determinants of prion conversion is critical to predicting the susceptibility of a species to infection.

The mammalian prion protein consists of ~210 amino acids arranged in a disordered amino-terminal tail and a globular C-terminal domain composed of three $\alpha$-helices and a short anti-parallel $\beta$-sheet (10, 11). Prion disease develops when a $\beta$-sheet-rich prion protein aggregate, known as $PrP^{Sc}$, recruits and templates the conversion of the normal cellular prion protein, $PrP^C$, in an autocatalytic process (12, 13). The primary structure of host $PrP^C$ profoundly impacts cross-species prion transmission; for example, a polymorphic site in sheep PrP influences susceptibility to classical sheep scrapie infection, in that sheep expressing PrP with Gln-168 or Arg-168 (human numbering (14)) are susceptible or resistant to infection, respectively (15, 16). Additionally, nearly all patients with variant Creutzfeldt-Jakob disease, likely due to bovine spongiform encephalopathy transmission to humans, encode a methionine at polymorphic codon 129 of the *PRNP* gene (17). Single residue substitutions in mouse $PrP^C$ have also been shown to reduce or prevent prion conversion *in vitro* (*e.g.* I139M (18), N155Y (19), Q168R (20, 21), Q219E (20), Q172R (22), and N174S (23) (human numbering (14)). Interestingly, several substitutions that inhibit prion formation are located within the $\beta$2-$\alpha$2 loop of PrP (residues 165–175), suggesting that the amino acid sequence of this region may impact prion conversion.

Microcrystal structures of select hexapeptide segments from the prion protein have revealed a cross-$\beta$ fibril spine consisting of pairs of tightly packed $\beta$-sheets aligned parallel to the fibril axis. In each sheet, segments form backbone hydrogen bonds with segments above and below them along the fibril axis.

* This work was supported, in whole or in part, by National Institutes of Health Grants NS076896, NS069566, and U54AI0359 (to C. J. S.) and AG029430 (to D. E.). This work was also supported by Morris Animal Foundation Fellowship D13ZO-419 (to T. D. K.).

[1] To whom correspondence should be addressed: Dept. of Pathology, University of California San Diego, 9500 Gilman Dr., La Jolla, CA 92093. Tel.: 858-534-0978; Fax: 858-246-0523; E-mail: csigurdson@ucsd.edu.

[2] The abbreviations used are: PrP, prion protein; MoPrP, mouse prion protein.

Between the two β-sheets, complementary side chains tightly interdigitate in a "steric zipper," forming a dry interface within the protofibril core (24, 25). Because this highly organized structure requires interdigitating side chains, heterologous PrP molecules with incompatible side chain interactions could sterically clash, which may explain the species barriers observed in prion disease (26, 27). For example, steric zipper segments composed of PrP residues 138–143 of hamster and human PrP crystallize into different space groups, with variation in the arrangement of β-strands and β-sheets (27). These differences in the preferred packing arrangements of the side chains, particularly at positions 138 and 139 (methionine and isoleucine) would probably lead to a steric clash for interacting segments of hamster and human PrP (27), in agreement with the poor fibrillization of a mixture of PrP segments (residues 23–144) having substitutions at positions 138 and 139 (28). The β2-α2 loop of PrP has also been crystallized and forms parallel β-sheets with side chains arranged in a steric zipper (24).

We previously demonstrated that residues 170 and 174 within the β2-α2 loop act as a molecular switch in transgenic mice expressing mouse PrP with S170N and N174T substitutions ($MoPrP^{170,174}$). Tg($MoPrP^{170,174}$) mice showed increased susceptibility to chronic wasting disease and hamster prions as compared with mice expressing wild type (WT) mouse PrP (MoPrP) (29). The secondary structure of the $MoPrP^{170,174}$ variant shows a well defined, "rigid" β2-α2 loop, whereas the WT MoPrP loop is disordered by NMR spectroscopy (30). Thus, the altered susceptibility observed in Tg($MoPrP^{170,174}$) mice could have been due to a difference in the primary structure or to the variant loop conformation. Interestingly, transgenic mice expressing mouse PrP with the D167S substitution ($MoPrP^{167}$), which also results in a well defined β2-α2 loop by NMR (31), show no detectable change in species barriers (32), suggesting that the PrP primary sequence may override the secondary structure in promoting prion conversion.

Within the β2-α2 loop (166–175), only 3 residues are strictly conserved, Tyr-169, Gln-172, and Asn-173 (33, 34). NMR structural studies have shown that a Y169G substitution modifies the loop structure from a $3_{10}$-helix turn to a type-1 β-turn (35). We recently found that transgenic mice expressing MoPrP having the Y169G substitution together with the S170N and N174T substitutions completely resist infection with either mouse or deer prions, implicating tyrosine 169 as critical for prion conversion (36). We set out to test how amino acid side chains at position 169 influence conversion and to then consider our results in the context of atomic level models of $PrP^{Sc}$ structure. Here, we performed a series of *in vitro* prion conversion experiments in which diverse amino acids were substituted at position 169 of mouse PrP. We found robust differences in prion conversion among the $PrP^{C}$ variants, and we propose a structural model based on amino acid side chain interactions within a steric zipper comprising PrP residues 167–176 to explain these results.

## EXPERIMENTAL PROCEDURES

*Prion Conversion Using PrP Mutants as Substrates*—Mouse *Prnp* cDNA containing the rigid loop mutations (corresponding to S170N and N174T) was subcloned into the pcDNA3.1C vector (Invitrogen). Site-directed mutagenesis was performed to obtain WT-pcDNA3.1C and to introduce the 3F4 tag (residues Met-109 and Met-112, human PrP numbering) into the PrP sequence. Further site-directed mutagenesis (Agilent) was performed to generate mouse *Prnp* encoding PrP with various amino acid substitutions. Mutations in the *Prnp* sequence were confirmed by DNA sequencing.

Confluent RK13 cells were transfected with plasmids using Lipofectamine 2000 (Invitrogen). At 24 h post-transfection, cells were washed twice and harvested in 1 ml of PBS. Cells were then centrifuged at 1000 × *g* for 1 min, and the pellet was resuspended in PMCA buffer (PBS containing 1% Triton X-100 and 0.05% saponin) prior to being passed twice through a 27-gauge needle. The lysates were then centrifuged at 2000 × *g* for 1 min, the pellets were discarded, and protein concentrations of the supernatants were measured by a bicinchoninic acid assay.

To seed the lysates, 5 μl of a 10% prion-infected brain homogenate in PBS was added to 45 μl of RK13 cell lysates in 0.2-ml PCR tubes. Tubes were then positioned in a microplate sonicator (QSonica S-4000) programmed to perform repeated cycles of 10-min incubation at 37 °C followed by a 5-s pulse of sonication at potency 50–60%. After 24 h, samples were digested with 100 μg/ml proteinase K for 30 min at 37 °C and analyzed by SDS-PAGE. Undigested samples for comparison of $PrP^{C}$ levels in different lysates consisted of 1.5 μl from unseeded samples.

*Western Blot and Quantification of PrP Signal*—Immunoblotting was performed using the anti-PrP antibody 3F4 (37) followed by HRP-conjugated anti-mouse secondary antibody. Signals were captured and quantified using a Fujifilm LAS-4000 imager and Multi Gauge software. For quantification of conversion efficiency, the ratio of proteinase K-resistant PrP to total $PrP^{C}$ was calculated and compared with WT samples according to the formula, $((PrP^{Sc}/PrP^{C})_{mutant}/(PrP^{Sc}/PrP^{C})_{WT}) \times 100$. The conversion products were easily distinguished from the $PrP^{Sc}$ seed with the 3F4 antibody because the 3F4 epitope is not present in mouse $PrP^{Sc}$. Unseeded controls were included in all experiments to evaluate the $PrP^{C}$ mutants for proteinase K-resistant PrP that may develop from self-aggregation. At least three experimental replicates were performed.

*Modeling β2-α2 Loop Steric Zippers*—In order to explore structural models of prion conversion at the β2-α2 loop, the zipper structure of PrP peptide 167–176 was built using Rosetta (38). The segment 167–176 was modeled as a parallel β-sheet. The pair of β-sheets was assembled by exploring all four possible arrangements (class 1–4). The zipper structure of PrP(167–176) was refined by simultaneously optimizing the rigid body degree of freedom between the β-sheets, side chain, and backbone torsions of each β-strand, guided by full-atom Rosetta energy functions (39). Taking advantage of the recently developed symmetry implementation in Rosetta (40), the fibril symmetry of each peptide subunit was restrained to assure that symmetrical geometry was satisfied during the whole optimization process. Finally, the models were inspected based on Rosetta energy and the packing between β-sheets, and the final zipper models with strong predicted zipper energy were selected. A class 4 zipper arrangement, highly similar to the

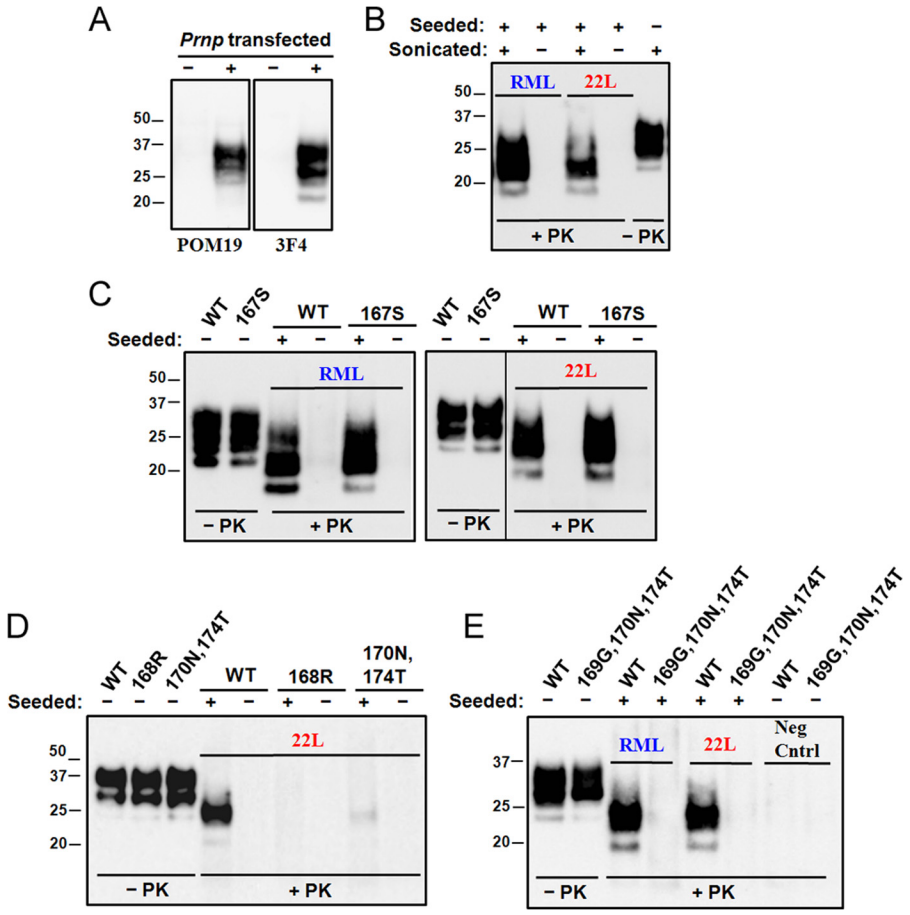


FIGURE 1. **Prion conversion using mutant PrP-expressing cells replicates *in vivo* prion susceptibility.** *A*, $PrP^C$ was only detected in RK13 cell lysates after transfection with *Prnp* plasmids. Anti-PrP monoclonal antibodies used were 3F4 (*right*), which recognizes the 3F4 epitope (residues 109–112), or POM19 (*left*), which recognizes various mammalian $PrP^C$ structures (53). POM19 labeling shows that untransfected RK13 cells lack detectable $PrP^C$. *B*, RK13 cell lysates expressing WT $PrP^C$ were seeded with RML or 22L prions and were either subjected to cycles of sonication at 37 °C (*lanes 1* and *3*) or were frozen (*lanes 2* and *4*). *C*, $PrP^C$ containing the Ser-167 substitution was efficiently converted by RML and 22L prions (RML, 127 ± 10%; 22L, 160 ± 42%) (mean ± S.E.) compared with WT mouse $PrP^C$. *D*, conversion of $PrP^C$ containing the Arg-168 or Asn-170/Thr-174 substitutions was minimal compared with WT mouse $PrP^C$ (for Arg-168, RML was 10 ± 4% and 22L was 5 ± 1%; for Asn-170/Thr-174, RML was 4 ± 1% and 22L was 7 ± 2%). *E*, conversion of $PrP^C$ containing the Y169G and S170N/N174T substitutions was scarcely detectable as compared with WT mouse $PrP^C$ (RML, 6 ± 1%; 22L, 3 ± 0%). $PrP^C$ levels were uniform among the samples (−*PK lanes*). *PK*, proteinase K. Data are representative of at least three independent experiments. Quantification is an average of all experiments performed for each mutant PrP.

recently determined atomic structure of PrP(171–176) peptide fibrils,[3] was most consistent with our experimental data.

## RESULTS

To assess the effect of residue substitutions on $PrP^C$ to $PrP^{Sc}$ conversion, we performed seeded conversion experiments using $PrP^C$ derived from cell lysates as a substrate and $PrP^{Sc}$ from prion-infected brain homogenate as a seed as described recently (22, 41, 42). $PrP^C$-deficient RK13 cells (Fig. 1*A*, *left*) were transfected with a plasmid encoding mouse PrP with the 3F4 epitope tag, which is recognized by the 3F4 antibody (3F4 residues 109–112, MKHM) (Fig. 1*A*, *right*) (41, 43, 44). Similar to protein-misfolding cyclic amplification (45), the mixtures of $PrP^C$ and $PrP^{Sc}$ were subjected to 24 h of intermittent bursts of sonication followed by incubation at 37 °C. $PrP^C$ containing the 3F4 epitope was readily converted by mouse prions, and the mouse $PrP^{Sc}$ seed was not detected in the unsonicated control samples (Fig. 1*B*). Thus, the newly converted, proteinase K-resistant $PrP^{Sc}$ could be readily identified by Western blotting. Two mouse prion strains, RML and 22L, were used to seed conversion of $PrP^C$. RML and 22L strains are distinguished by their differing incubation period and brain lesion distribution in mice (46).

*In Vitro Prion Conversion Assay Correlates with in Vivo Susceptibility*—To assess whether the RK13 cell-derived PrP conversion assay reproduced known transmission barriers, we measured the conversion of mutant $PrP^C$ from *in vivo* models. In transgenic mouse models, the D167S substitution did not impact the susceptibility of mice to RML prions (32). Consistent with *in vivo* findings, here we found that the D167S substitution also had no impact on *in vitro* conversion by RML or 22L mouse prions (Fig. 1*C*). In contrast, transgenic mice expressing the Q168R substitution are protected from prion infection (21), and similarly, the Q168R substitution blocked *in vitro* conversion by RML or 22L prions in the prion conversion assay (Fig. 1*D*). Furthermore, conversion of $PrP^C$ containing the S170N and N174T substitutions was reduced to only 4–7% (Figs. 1*D* and 2*A*), analogous to

[3] H. MacFarlane and D. Eisenberg, unpublished data.

**TABLE 1**
***In vitro* prion conversion assay correlates with *in vivo* susceptibility**

| $PrP^C$ sequence | Inoculum | Attack rate *in vivo* (reference) | In vitro conversion relative to WT $PrP^C$ (Mean ± S.E.) |
|---|---|---|---|
| | | | % |
| $MoPrP^{D167S}$ | RML | 100% (32) | 127 ± 10 |
| $MoPrP^{Q168R}$ | RML | 0% (21) | 10 ± 4 |
| $MoPrP^{170,174}$ | RML | 100% (29)[a] | 4 ± 1 |
| $MoPrP^{169,170,174}$ | RML | 0% (36) | 6 ± 1 |

[a] Although the attack rate is 100%, Tg($MoPrP^{170,174}$) mice express $PrP^C$ at approximately 2–3-fold WT levels and have incubation periods more than 2-fold longer than WT mice, suggesting a significant barrier to infection with RML prions.

Tg($MoPrP^{170,174}$) mice that show a barrier to infection with mouse prions.

We recently showed that mice expressing three substitutions in the β2-α2 loop at positions 169, 170, and 174 completely resist infection with mouse prions (RML and 22L) and deer prions (chronic wasting disease) (36). Here we found that the same substitutions (Y169G, S170N, and N174T) reduced *in vitro* conversion by RML and 22L to only 3–6% of the levels observed with WT mouse $PrP^C$ (Fig. 1*E*). These data indicate that the prion conversion assay accurately reflects the *in vivo* susceptibility of transgenic mice to prion infection (Table 1).

*Single β2-α2 Loop Residue Substitutions Differ in Their Impact on Prion Conversion*—The Y169G, S170N, and N174T residues inhibited prion conversion; however, the contribution of each substitution to the transmission barrier observed in the Tg($MoPrP^{169,170,174}$) mice could not be determined. To quantify how each β2-α2 loop substitution perturbed prion conversion, we performed the conversion assay using $PrP^C$ substrate having a single substitution. The N174T substitution reduced conversion by 22L or RML mouse prions to ~40% (Fig. 2*A*). The S170N substitution similarly reduced conversion by 22L to ~50% (Fig. 2*B*, *bottom*) but had little effect on conversion by RML prions (Fig. 2*B*, *top*), consistent with previous reports (18). Interestingly, we found that the single Y169G substitution had the most profound effect, reducing conversion by 22L and RML to just 20–25% relative to the WT mouse sequence (Fig. 2*B*).

*An Aromatic Residue at Position 169 Is Required for PrP Conversion*—To further assess whether an aromatic amino acid at position 169 promotes prion conversion, we performed seeded conversion using mouse $PrP^C$ containing a Y169F or Y169W substitution. In contrast to Y169G, the 169F or 169W substitutions readily supported conversion by mouse prions at levels equivalent to conversion of WT mouse $PrP^C$ (Fig. 3*A*). In contrast, substitution of a polar residue, glutamine, or a hydrophobic residue, leucine, at position 169 reduced prion conversion to only 25% of WT levels (Fig. 3*B*), similar to the Y169G. Collectively, these results suggest that an aromatic or bulky residue having a large side chain at position 169 is essential for efficient conversion by mouse prions *in vitro*.

*Steric Constraints on $PrP^{Sc}$ Structure*—The crystal structures of steric zipper segments of the prion protein provide insight into well known prion species barriers, such as the mouse and hamster. On the basis of these structures, the mouse and hamster 138–143 segments are predicted to be incompatible for forming a steric zipper due to a steric clash between the side chains of residues 138 and 139 (27). The PrP peptides 170–175 and 171–176 have also been crystallized and shown to form steric zipper structures, a common motif for the spine of amyloid fibers in which a pair of β-sheets is held together by side chain interdigitation (24, 26, 47).

Based on the crystal structure of the 170–176 segment of mouse PrP (a class 4 steric zipper) (24)[3] ((Fig. 4*A*), we modeled the side chain interactions between $PrP^C$ segments containing the Q168R or S170N and N174T substitutions. Neither the Q168R nor the S170N/N174T variant segments would be expected to form a steric zipper with mouse PrP due to steric clashes in the interacting amino acid side chains, which may explain the poor conversion of these PrP mutants in the seeded conversion assay (Fig. 4, *B* and *C*). In contrast, the D167S substitution is sterically compatible with mouse $PrP^C$ in the zipper structure (Fig. 4*D*).

To better understand how a bulky residue at position 169 may enhance PrP conversion, we aligned the mouse segment with the mouse variants and examined whether the side chains can interdigitate at the β-sheet interface using structural modeling methods (Fig. 4). The Y169G, Y169L, and Y169Q substitutions (Fig. 4, *E*–*G*) resulted in a cavity between the β-sheets, which indicates poor packing. This loose fit between the side chains could explain the inefficient seeding and conversion of these PrP mutants by WT mouse prions. In contrast, the Phe-169 and Trp-169 residues (Fig. 5, *H* and *I*) fill the space normally occupied by the tyrosine side chain, which results in tight interdigitation between side chains and a complementary steric zipper between residues 167 and 176 of these PrP peptide variants and mouse PrP.

We modeled other amino acid substitutions at position 169, including histidine, isoleucine, and valine. The zipper models formed by these residues contain a cavity, suggesting that they would not support efficient prion conversion. Calculations of the predicted zipper energies suggest that formation of a zipper containing His, Ile, Val, Leu, Gly, or Gln at position 169 would be less energetically favorable than Tyr. In contrast, the predicted energy for formation of a zipper containing Trp or Phe at position 169 is comparable with that of Tyr. Taken together, our experimental results on prion conversion are compatible with the steric zipper model.

## DISCUSSION

Recruitment of monomeric $PrP^C$ into β-sheet-rich $PrP^{Sc}$ requires sequence similarity, and certain residues obstruct conversion (20, 22, 48). Adhesive segments of the prion protein may contain key residues that contribute to the stability of a β-sheet (24). One such segment in PrP was identified as the β2-α2 loop, which is rich in asparagine, glutamine, and tyrosine residues that could provide increased hydrogen bonding between β-strands (24, 25). Single substitutions within the β2-α2 loop can inhibit prion conversion (20, 22, 48, 49), yet the molecular mechanism underlying the inhibition is unclear. Previous work indicates that transgenic mice expressing WT $PrP^C$ with substitutions at loop positions 169, 170, and 174 resist infection with prions from mice and deer (36). Using the *in vitro* cell-free conversion assay to test the individual 169, 170, and 174 substitutions, we found that Y169G had the most pronounced effect on prion conversion.

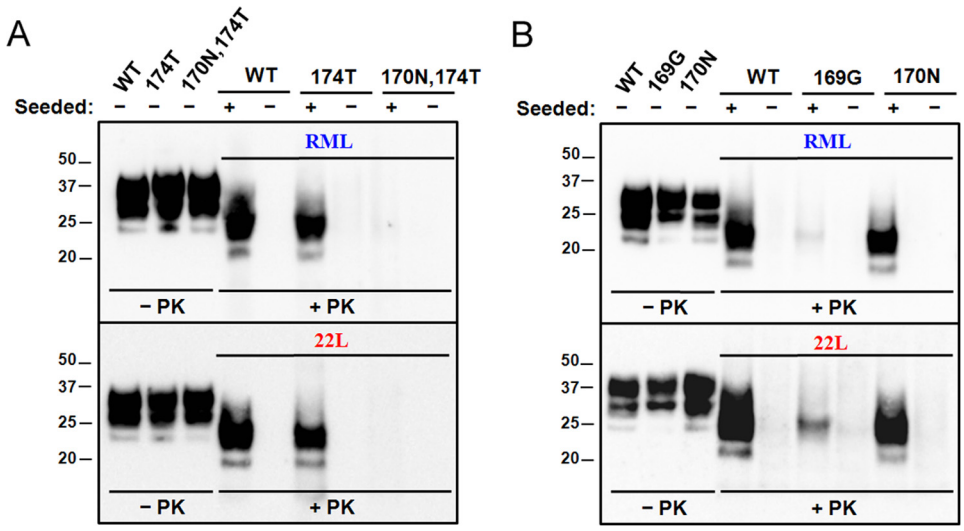


FIGURE 2. **The Y169G substitution in PrP$^{C}$ reduces conversion by mouse prions.** *A*, mouse PrP$^{C}$ containing both the S170N and N174T substitutions was converted much less efficiently compared with the N174T substitution (for N174T, RML was 35 ± 13% and 22L was 44 ± 13%). *B*, mouse PrP$^{C}$ containing the Y169G substitution revealed poor conversion (RML, 25 ± 15%; 22L, 21 ± 6%) compared with the S170N substitution (RML, 124 ± 39%; 22L, 51 ± 12%).

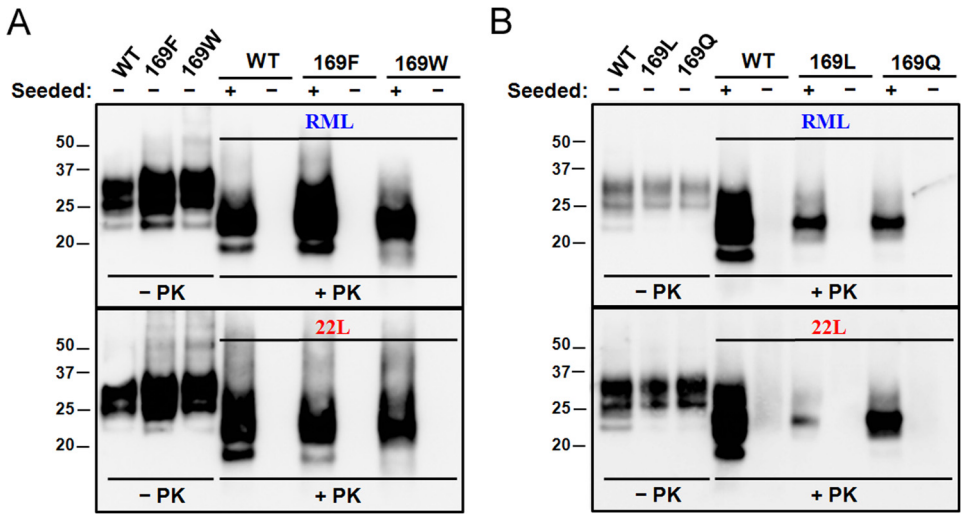


FIGURE 3. **An aromatic amino acid side chain at position 169 of PrP$^{C}$ is essential for efficient prion conversion.** *A*, PrP$^{C}$ containing either the Phe-169 or Trp-169 substitution was efficiently converted by RML or 22L (for Phe-169, RML was 122 ± 40% and 22L was 117 ± 7; for Trp-169, RML was 95 ± 24% and 22L was 117 ± 37). *B*, conversion of PrP$^{C}$ containing the Leu-169 or Gln-169 substitutions was poor (For Leu-169, RML was 26 ± 6% and 22L was 11 ± 2; for Gln-169, RML was 24 ± 6%, and 22L was 26 ± 8%).

How does the Y169G substitution inhibit prion conversion? The strictly conserved Tyr-169 has a key role in maintaining the $3_{10}$-helical turn in the $\beta$2-$\alpha$2 loop, and the Y169G substitution results in the loss of a $\pi$-stacking interaction with 175F and a switch to a type I $\beta$-turn, forming a well defined loop (35, 50, 51). The new loop orientation may obstruct PrP$^{C}$-PrP$^{Sc}$ interactions, preventing efficient binding and conversion. However, we have found that two MoPrP$^{C}$ variants, MoPrP$^{D167S}$ and MoPrP$^{S170N,N174T}$, both transform the disordered $\beta$2-$\alpha$2 loop into a well defined "rigid loop" structure yet have opposing effects on species barriers; the MoPrP$^{D167S}$ causes no detectable impact on species barriers, whereas the MoPrP$^{S170N/N174T}$ substitutions have a major impact on species barriers. We also report here that the MoPrP$^{Y225A}$ variant, which shows a well defined $\beta$2-$\alpha$2 loop by NMR (52), was efficiently converted by mouse prions (Fig. 5). Thus, prion conversion may require certain compatible features in the primary structures of PrP that override secondary structural differences, and further studies will aid in distinguishing between these possibilities.

A second possible structural explanation for the strong impact of the Y169G and other non-aromatic amino acid substitutions on prion conversion is the altered side chain interactions of residues 165–175 predicted to occur within a $\beta$-sheet. The atomic structure of crystallized PrP peptide fibrils encompassing amino acids 170–175 has been well characterized (27) and forms the basis of the models proposed here (Fig. 4). The models are consistent with our experimental data, in which the size of the side chains at position 169 contributes to prion conversion efficiency. Bulky residues (Phe, Tyr, and Trp) at position 169 could facilitate prion conversion by providing maximum hydrophobic contacts and tighter shape complementarity at zipper interfaces, whereas residues with either hydrophobic or hydrophilic side chains (such as Leu or Gln) could not support conversion because they offer fewer residue contacts and

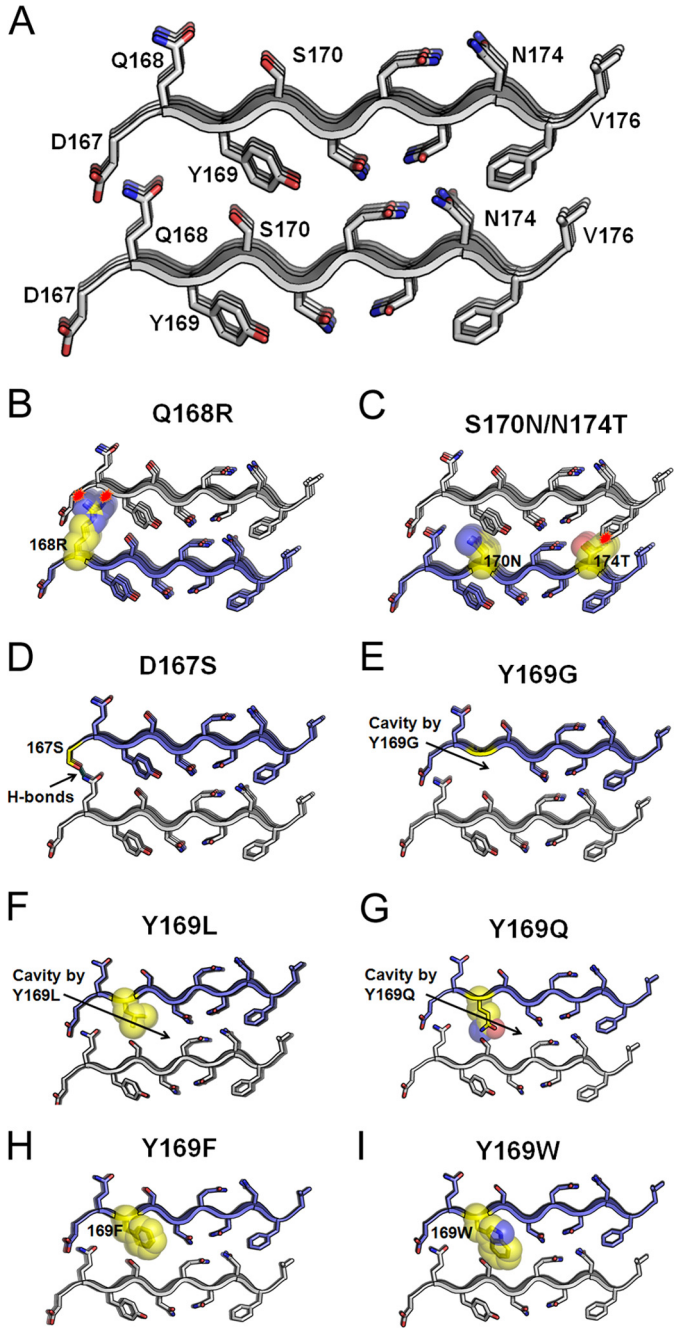


FIGURE 4. **Steric zipper models support the role of side chain steric compatibility in prion conversion.** *A*, zipper model of the PrP(167–176) fibril shows the WT sequence of the mouse, DQYSNQNNFV. In this low energy model, the pair of $\beta$-sheets adopts a parallel, face-to-back arrangement (class 4 steric zipper). *B–I*, zipper models of wild type PrP (*gray*) and mutant PrP peptides (*blue*) highlight the compatibility between the two strands. Mutants shown are Q168R (*B*), S170N/N174T (*C*), D167S (*D*), Y169G (*E*), Y169L (*F*), Y169Q (*G*), Y169F (*H*), and Y169W (*I*).

result in poor packing at zipper interfaces. Whether other transmission barriers can be explained by the steric zipper at 170–175 remains to be seen.

Although the seeded prion conversion assay does not report the absolute susceptibility of a species to prion disease, the assay enables a comparison of how specific residue substitutions singly or in combination impact conversion relative to the WT sequence using post-translationally modified PrP. This work

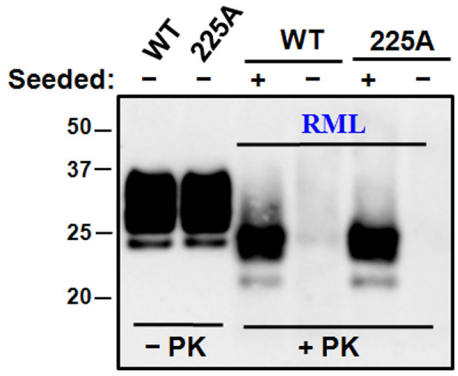


FIGURE 5. **The Y225A substitution in $PrP^C$ has no effect on prion conversion efficiency.** The mouse PrP variant containing the Y225A substitution has a well defined, "rigid" $\beta$2-$\alpha$2 loop conformation by NMR analysis (52). Mouse $PrP^C$ containing the Y225A substitution was converted by RML mouse prions as efficiently as WT $PrP^C$ (RML, 112 ± 9%; 22L, 111 ± 15%).

together with previous findings by our laboratory and others demonstrates that residues within the $\beta$2-$\alpha$2 loop may modulate susceptibility to prion disease. Because multiple steric zipper segments have been identified in PrP, including the $\beta$2-$\alpha$2 loop (24, 26, 27), different $PrP^{Sc}$ aggregates may have different zipper segments exposed, and thus the $PrP^C$-$PrP^{Sc}$ interacting segments may shift depending on the $PrP^{Sc}$ conformation. Additionally, the packing arrangement within a single zipper may alter the side chains that interact (25). It will be of great interest to further investigate how the exposed segments and the side chain packing arrangements in distinct $PrP^{Sc}$ conformations impact species barriers in prion disease.

*Acknowledgments—We thank Jun Liu for excellent technical support and Dr. Adriano Aguzzi for generously providing the anti-PrP antibody, POM19.*

## REFERENCES

1. Kirkwood, J. K., and Cunningham, A. A. (1994) Epidemiological observations on spongiform encephalopathies in captive wild animals in the British Isles. *Vet. Rec.* **135,** 296–303
2. Taylor, D. M. (1993) Bovine spongiform encephalopathy and its association with the feeding of ruminant-derived protein. *Dev. Biol. Stand.* **80,** 215–224
3. Ministry of Agriculture, Fisheries and Food (2000) *Bovine Spongiform Encephalopathy in Great Britain: A Progress Report*, p. 71, Ministry of Agriculture, Fisheries and Food, London
4. Bons, N., Mestre-Frances, N., Charnay, Y., Salmona, M., and Tagliavini, F. (1996) Spontaneous spongiform encephalopathy in a young adult rhesus monkey. *C. R. Acad. Sci. III* **319,** 733–736
5. Heisey, D. M., Mickelsen, N. A., Schneider, J. R., Johnson, C. J., Johnson, C. J., Langenberg, J. A., Bochsler, P. N., Keane, D. P., and Barr, D. J. (2010) Chronic wasting disease (CWD) susceptibility of several North American rodents that are sympatric with cervid CWD epidemics. *J. Virol.* **84,** 210–215
6. Perrott, M. R., Sigurdson, C. J., Mason, G. L., and Hoover, E. A. (2013) Mucosal transmission and pathogenesis of chronic wasting disease in ferrets. *J. Gen. Virol.* **94,** 432–442
7. Mitchell, G. B., Sigurdson, C. J., O'Rourke, K. I., Algire, J., Harrington, N. P., Walther, I., Spraker, T. R., and Balachandran, A. (2012) Experimental oral transmission of chronic wasting disease to reindeer (*Rangifer tarandus tarandus*). *PLoS One* **7,** e39055
8. Baeten, L. A., Powers, B. E., Jewell, J. E., Spraker, T. R., and Miller, M. W. (2007) A natural case of chronic wasting disease in a free-ranging moose

(*Alces alces shirasi*). *J. Wildl. Dis.* **43,** 309–314
9. Kreeger, T. J., Montgomery, D. L., Jewell, J. E., Schultz, W., and Williams, E. S. (2006) Oral transmission of chronic wasting disease in captive Shira's moose. *J. Wildl. Dis.* **42,** 640–645
10. Riek, R., Hornemann, S., Wider, G., Billeter, M., Glockshuber, R., and Wüthrich, K. (1996) NMR structure of the mouse prion protein domain PrP (121–231). *Nature* **382,** 180–182
11. Riek, R., Hornemann, S., Wider, G., Glockshuber, R., and Wüthrich, K. (1997) NMR characterization of the full-length recombinant murine prion protein, mPrP(23–231). *FEBS Lett.* **413,** 282–288
12. Prusiner, S. B., McKinley, M. P., Bowman, K. A., Bolton, D. C., Bendheim, P. E., Groth, D. F., and Glenner, G. G. (1983) Scrapie prions aggregate to form amyloid-like birefringent rods. *Cell* **35,** 349–358
13. Prusiner, S. B. (1982) Novel proteinaceous infectious particles cause scrapie. *Science* **216,** 136–144
14. Schätzl, H. M., Da Costa, M., Taylor, L., Cohen, F. E., and Prusiner, S. B. (1997) Prion protein gene variation among primates. *J. Mol. Biol.* **265,** 257
15. Hunter, N., Goldmann, W., Benson, G., Foster, J. D., and Hope, J. (1993) Swaledale sheep affected by natural scrapie differ significantly in PrP genotype frequencies from healthy sheep and those selected for reduced incidence of scrapie. *J. Gen. Virol.* **74,** 1025–1031
16. Hunter, N., Goldmann, W., Foster, J. D., Cairns, D., and Smith, G. (1997) Natural scrapie and PrP genotype: case-control studies in British sheep. *Vet. Rec.* **141,** 137–140
17. Mackay, G. A., Knight, R. S., and Ironside, J. W. (2011) The molecular epidemiology of variant CJD. *Int. J. Mol. Epidemiol. Genet.* **2,** 217–227
18. Priola, S. A., and Chesebro, B. (1995) A single hamster PrP amino acid blocks conversion to protease-resistant PrP in scrapie-infected mouse neuroblastoma cells. *J. Virol.* **69,** 7754–7758
19. Priola, S. A., Chabry, J., and Chan, K. (2001) Efficient conversion of normal prion protein (PrP) by abnormal hamster PrP is determined by homology at amino acid residue 155. *J. Virol.* **75,** 4673–4680
20. Kaneko, K., Zulianello, L., Scott, M., Cooper, C. M., Wallace, A. C., James, T. L., Cohen, F. E., and Prusiner, S. B. (1997) Evidence for protein X binding to a discontinuous epitope on the cellular prion protein during scrapie prion propagation. *Proc. Natl. Acad. Sci. U.S.A.* **94,** 10069–10074
21. Perrier, V., Kaneko, K., Safar, J., Vergara, J., Tremblay, P., DeArmond, S. J., Cohen, F. E., Prusiner, S. B., and Wallace, A. C. (2002) Dominant-negative inhibition of prion replication in transgenic mice. *Proc. Natl. Acad. Sci. U.S.A.* **99,** 13079–13084
22. Geoghegan, J. C., Miller, M. B., Kwak, A. H., Harris, B. T., and Supattapone, S. (2009) Trans-dominant inhibition of prion propagation *in vitro* is not mediated by an accessory cofactor. *PLoS Pathog.* **5,** e1000535
23. Vorberg, I., Groschup, M. H., Pfaff, E., and Priola, S. A. (2003) Multiple amino acid residues within the rabbit prion protein inhibit formation of its abnormal isoform. *J. Virol.* **77,** 2003–2009
24. Sawaya, M. R., Sambashivan, S., Nelson, R., Ivanova, M. I., Sievers, S. A., Apostol, M. I., Thompson, M. J., Balbirnie, M., Wiltzius, J. J., McFarlane, H. T., Madsen, A. Ø., Riekel, C., and Eisenberg, D. (2007) Atomic structures of amyloid cross-$\beta$ spines reveal varied steric zippers. *Nature* **447,** 453–457
25. Eisenberg, D., and Jucker, M. (2012) The amyloid state of proteins in human diseases. *Cell* **148,** 1188–1203
26. Apostol, M. I., Sawaya, M. R., Cascio, D., and Eisenberg, D. (2010) Crystallographic studies of prion protein (PrP) segments suggest how structural changes encoded by polymorphism at residue 129 modulate susceptibility to human prion disease. *J. Biol. Chem.* **285,** 29671–29675
27. Apostol, M. I., Wiltzius, J. J., Sawaya, M. R., Cascio, D., and Eisenberg, D. (2011) Atomic structures suggest determinants of transmission barriers in mammalian prion disease. *Biochemistry* **50,** 2456–2463
28. Vanik, D. L., Surewicz, K. A., and Surewicz, W. K. (2004) Molecular basis of barriers for interspecies transmissibility of mammalian prions. *Mol. Cell* **14,** 139–145
29. Sigurdson, C. J., Nilsson, K. P., Hornemann, S., Manco, G., Fernández-Borges, N., Schwarz, P., Castilla, J., Wüthrich, K., and Aguzzi, A. (2010) A molecular switch controls interspecies prion disease transmission in mice. *J. Clin. Invest.* **120,** 2590–2599
30. Gossert, A. D., Bonjour, S., Lysek, D. A., Fiorito, F., and Wüthrich, K. (2005) Prion protein NMR structures of elk and of mouse/elk hybrids. *Proc. Natl. Acad. Sci. U.S.A.* **102,** 646–650
31. Pérez, D. R., Damberger, F. F., and Wüthrich, K. (2010) Horse prion protein NMR structure and comparisons with related variants of the mouse prion protein. *J. Mol. Biol.* **400,** 121–128
32. Bett, C., Fernández-Borges, N., Kurt, T. D., Lucero, M., Nilsson, K. P., Castilla, J., and Sigurdson, C. J. (2012) Structure of the $\beta$2-$\alpha$2 loop and interspecies prion transmission. *FASEB J.* **26,** 2868–2876
33. Pastore, A., and Zagari, A. (2007) A structural overview of the vertebrate prion proteins. *Prion* **1,** 185–197
34. Wopfner, F., Weidenhöfer, G., Schneider, R., von Brunn, A., Gilch, S., Schwarz, T. F., Werner, T., and Schätzl, H. M. (1999) Analysis of 27 mammalian and 9 avian PrPs reveals high conservation of flexible regions of the prion protein. *J. Mol. Biol.* **289,** 1163–1178
35. Damberger, F. F., Christen, B., Pérez, D. R., Hornemann, S., and Wüthrich, K. (2011) Cellular prion protein conformation and function. *Proc. Natl. Acad. Sci. U.S.A.* **108,** 17308–17313
36. Kurt, T. D., Bett, C., Fernández-Borges, N., Joshi-Barr, S., Hornemann, S., Rülicke, T., Castilla, J., Wüthrich, K., Aguzzi, A., and Sigurdson, C. J. (2014) Prion transmission prevented by modifying the $\beta$2-$\alpha$2 loop structure of host PrPC. *J. Neurosci.* **34,** 1022–1027
37. Kascsak, R. J., Rubenstein, R., Merz, P. A., Tonna-DeMasi, M., Fersko, R., Carp, R. I., Wisniewski, H. M., and Diringer, H. (1987) Mouse polyclonal and monoclonal antibody to scrapie-associated fibril proteins. *J. Virol.* **61,** 3688–3693
38. Leaver-Fay, A., Tyka, M., Lewis, S. M., Lange, O. F., Thompson, J., Jacak, R., Kaufman, K., Renfrew, P. D., Smith, C. A., Sheffler, W., Davis, I. W., Cooper, S., Treuille, A., Mandell, D. J., Richter, F., Ban, Y. E., Fleishman, S. J., Corn, J. E., Kim, D. E., Lyskov, S., Berrondo, M., Mentzer, S., Popović, Z., Havranek, J. J., Karanicolas, J., Das, R., Meiler, J., Kortemme, T., Gray, J. J., Kuhlman, B., Baker, D., and Bradley, P. (2011) ROSETTA3: an object-oriented software suite for the simulation and design of macromolecules. *Methods Enzymol.* **487,** 545–574
39. Kuhlman, B., Dantas, G., Ireton, G. C., Varani, G., Stoddard, B. L., and Baker, D. (2003) Design of a novel globular protein fold with atomic-level accuracy. *Science* **302,** 1364–1368
40. André, I., Bradley, P., Wang, C., and Baker, D. (2007) Prediction of the structure of symmetrical protein assemblies. *Proc. Natl. Acad. Sci. U.S.A.* **104,** 17656–17661
41. Mays, C. E., Yeom, J., Kang, H. E., Bian, J., Khaychuk, V., Kim, Y., Bartz, J. C., Telling, G. C., and Ryou, C. (2011) *In vitro* amplification of misfolded prion protein using lysate of cultured cells. *PLoS One* **6,** e18047
42. Yokoyama, T., Takeuchi, A., Yamamoto, M., Kitamoto, T., Ironside, J. W., and Morita, M. (2011) Heparin enhances the cell-protein misfolding cyclic amplification efficiency of variant Creutzfeldt-Jakob disease. *Neurosci. Lett.* **498,** 119–123
43. Courageot, M. P., Daude, N., Nonno, R., Paquet, S., Di Bari, M. A., Le Dur, A., Chapuis, J., Hill, A. F., Agrimi, U., Laude, H., and Vilette, D. (2008) A cell line infectible by prion strains from different species. *J. Gen. Virol.* **89,** 341–347
44. Vilette, D., Andreoletti, O., Archer, F., Madelaine, M. F., Vilotte, J. L., Lehmann, S., and Laude, H. (2001) *Ex vivo* propagation of infectious sheep scrapie agent in heterologous epithelial cells expressing ovine prion protein. *Proc. Natl. Acad. Sci. U.S.A.* **98,** 4055–4059
45. Saborio, G. P., Permanne, B., and Soto, C. (2001) Sensitive detection of pathological prion protein by cyclic amplification of protein misfolding. *Nature* **411,** 810–813
46. Karapetyan, Y. E., Saá, P., Mahal, S. P., Sferrazza, G. F., Sherman, A., Salès, N., Weissmann, C., and Lasmézas, C. I. (2009) Prion strain discrimination based on rapid in vivo amplification and analysis by the cell panel assay. *PLoS One* **4,** e5730
47. Nelson, R., Sawaya, M. R., Balbirnie, M., Madsen, A. Ø., Riekel, C., Grothe, R., and Eisenberg, D. (2005) Structure of the cross-$\beta$ spine of amyloid-like fibrils. *Nature* **435,** 773–778
48. Atarashi, R., Sim, V. L., Nishida, N., Caughey, B., and Katamine, S. (2006) Prion strain-dependent differences in conversion of mutant prion proteins in cell culture. *J. Virol.* **80,** 7854–7862
49. Belt, P. B., Muileman, I. H., Schreuder, B. E., Bos-de-Ruijter, J., Gielkens,

A. L., and Smits, M. A. (1995) Identification of five allelic variants of the sheep PrP gene and their association with natural scrapie. *J. Gen. Virol.* **76,** 509–517

50. Christen, B., Damberger, F. F., Pérez, D. R., Hornemann, S., and Wüthrich, K. (2013) Structural plasticity of the cellular prion protein and implications in health and disease. *Proc. Natl. Acad. Sci. U.S.A.* **110,** 8549–8554
51. Christen, B., Hornemann, S., Damberger, F. F., and Wüthrich, K. (2012) Prion protein mPrP[F175A](121–231): structure and stability in solution. *J. Mol. Biol.* **423,** 496–502
52. Christen, B., Hornemann, S., Damberger, F. F., and Wüthrich, K. (2009) Prion protein NMR structure from tammar wallaby (*Macropus eugenii*) shows that the $\beta$2-$\alpha$2 loop is modulated by long-range sequence effects. *J. Mol. Biol.* **389,** 833–845
53. Polymenidou, M., Moos, R., Scott, M., Sigurdson, C., Shi, Y. Z., Yajima, B., Hafner-Bratkovic, I., Jerala, R., Hornemann, S., Wuthrich, K., Bellon, A., Vey, M., Garen, G., James, M. N., Kav, N., and Aguzzi, A. (2008) The POM monoclonals: a comprehensive set of antibodies to non-overlapping prion protein epitopes. *PLoS One* **3,** e3872